Isotropic Pressure-Densified Atactic Poly(methyl methacrylate) Glasses: Free-Volume Properties from Equation-of-State Data and Positron Annihilation Lifetime Spectroscopy

Marcus Schmidt[†] and Frans H. J. Maurer*[,‡]

Department of Polymer Technology, Chalmers University of Technology, SE-412 96 Göteborg, Sweden, and Department of Polymer Science & Engineering, Lund Institute of Technology, Center for Chemistry and Chemical Engineering, Lund University, SE-221 00 Lund, Sweden

Received October 19, 1999; Revised Manuscript Received February 11, 2000

ABSTRACT: We modified the sample cell of a commercial pressure−volume−temperature (*PVT*) apparatus to make glasses by pressure densification (0−200 MPa) in the equilibrium melt. The *PVT* data of the glasses and the melt were analyzed in terms of the Simha−Somcynsky equation-of-state (EOS) theory and the Tait EOS. Small macroscopic volume changes up to 1.2% were found to yield large microscopic volume changes in isotropic pressure-densified atactic poly(methyl methacrylate) glasses with densities in the range 1.1823−1.1963 g/cm^3: the free-volume fraction h from the Simha−Somcynsky theory decreased by up to 19.2%, the orthopositronium (o-Ps) lifetime τ_3 from positron annihilation lifetime spectroscopy (PALS) decreased by up to 8.4% whereas the o-Ps intensity I_3 remained constant at 29 ± 0.5%, and the volume of the free-volume cavities $V(\tau_3)$ decreased by up to 16.1%. Moreover, the microscopic volume quantities h and $V(\tau_3)$ were found to correlate best. The radius of the free-volume cavities $R(\tau_3)$ at zero h appears to approach the Bohr radius of the o-Ps species. The thermal expansivity α_0 remains almost constant, the isothermal compressibility κ_0 decreases by up to 10.3%, which corresponds to an 11.5% increase in bulk modulus, and the freezing fraction remains constant up to formation pressures of 200 MPa.

Introduction

The volume and free volume of a polymer glass depend on its thermodynamic formation history. A polymer glass can be densified in essentially five different ways as illustrated schematically in Figure 1: that is, by isothermally compressing the glass, as is common in pressure−volume−temperature (*PVT*) analysis[1−4] (path A→A′ for a glass formed at atmospheric pressure along P_0→B→A, where B is the glass transition T_g at atmospheric pressure); by volume relaxation of the glass due to physical aging[5,6] (path A→a_i following a temperature quench from P_0→A); by decreasing the cooling rate r_c from the equilibrium melt to the glass[7,8] (path P_0→B→$T_g(r_c)$→a_i, where the suppressed glass transition $T_g(r_c)$ lies below B and $T_g(r_c)$→a_i lies parallel to B→A); by pressurizing the melt until it vitrifies at a glass formation pressure P_d at the pressure-dependent and formation pressure-dependent glass transition temperature $T_g^*(P,P_d)$[9] and followed by cooling of the glass and then releasing the pressure (path b→b_i→B_i→A_i→a_i, where $b_i = P_d$); and by cooling the melt under pressure P_i to below the pressure-dependent $T_g(P)$ and then releasing the pressure (path P_0→P_i→B_i→A_i→a_i or path P_0→P_i→P_{i+1}→B_{i+1}→A_{i+1}→a_{i+1} for even higher densification pressures $P_d = P_{i+1}$). In the literature, the latter two are often referred to as pressure densification to distinguish them from the three other possible densifications. At infinitely slow cooling rates and pressurization rates, both pressure-densification paths b→b_i→B_i→A_i→a_i and P_0→P_i→B_i→A_i→a_i should yield identical glasses. In practice, however, pressurization rates often exceed cooling rates, and because the polymer flows during both pressurization steps b→b_i and P_0→P_i, the melt can vitrify free from orientations and internal stresses in the cooling step of the latter compared with crossing $T_g^*(P,P_d)$ in the former. This

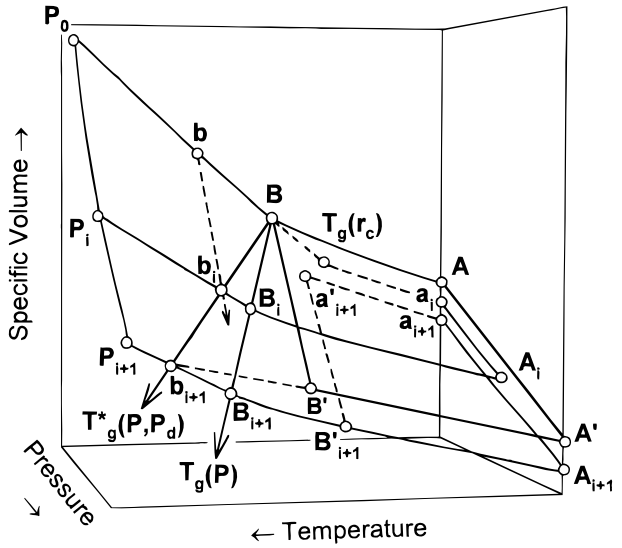

Figure 1. Schematic illustration of the *PVT* surface of an amorphous polymer. The different densification paths are explained in the text. B→P_0→P_i→P_{i+1}→B_{i+1}→B is the equilibrium melt surface, and A→B→B′→A′→A and a_{i+1}→a'_{i+1}→B'_{i+1}→A_{i+1}→a_{i+1} are glass surfaces obtained by cooling from the melt to below the pressure-dependent glass transition temperature $T_g(P)$ at formation or densification pressures of $P_d = P_0$ and $P_d = P_{i+1}$, respectively. Each glassy surface intersects the equilibrium melt surface with its own characteristic glass transition temperature $T_g^*(P,P_d)$ that is dependent on both pressure and formation pressure. A typical pressure-densification cycle is A→B→P_0→P_i→B_i→A_i→a_i for a densification pressure P_i (i = 0−4). P_0→P_i and A_i→a_i are pressurization and depressurization steps, respectively.

† Chalmers University of Technology.
‡ Lund Institute of Technology.
* To whom correspondence should be addressed. Fax +46-46-2224115; e-mail frans.maurer@polymer.lth.se.

10.1021/ma991722h CCC: $19.00
Published on Web 04/21/2000

has actually been observed in densification studies of polystyrene (PS)[10] and may account for some of the nonlinear density changes with P_d reported in the literature. Thus, $P_0 \rightarrow P_i \rightarrow B_i \rightarrow A_i \rightarrow a_i$ is the preferred path for pressure densification studies. It should be noted that every P_d yields a glass with a different *PVT* surface, as shown in Figure 1, by the surfaces $A \rightarrow B \rightarrow B' \rightarrow A' \rightarrow A$ and $a_{i+1} \rightarrow a'_{i+1} \rightarrow B'_{i+1} \rightarrow A_{i+1} \rightarrow a_{i+1}$ for $P_d = P_0$ and $P_d = P_{i+1}$, respectively. Each glassy surface intersects the equilibrium melt surface $B \rightarrow P_0 \rightarrow P_i \rightarrow P_{i+1} \rightarrow B_{i+1} \rightarrow B$ with its own characteristic line of intersection $T_g^*(P,P_d)$. Pressure densification can be achieved within a few hours, whereas slow cooling from the melt at atmospheric pressure would take about 200 years to obtain the same densification as estimated in the case of poly(vinyl acetate) (PVAc).[11] Depending on the formation pressure and polymer, the volume changes associated with pressure-densified polymer glasses are typically 1−2% and exceed those that accompany physical aging by 1−2 orders of magnitude.[5] In physical aging, the time needed to approach thermodynamic equilibrium increases by about 1 decade for every 3 °C below T_g compared with about 100 s at T_g.[5] It can be readily shown that voluminal equilibrium at room temperature would be reached only after about 8 months for PVAc and would be practically impossible for poly(methyl methacrylate) (PMMA). Thus, physical aging is both impractical and impossible for making densified glasses with relatively large densifications. Since the early reports on pressure densification of inorganic and low molecular weight organic glasses by Tammann and Jenckel,[12] most studies have dealt with *PVT*,[10,11,13−34] thermodynamic,[9,10,16,17,19,21−24,27−30,35−38] mechanical,[10,23,25,28,39] dielectric,[15,28,40,41] and viscoelastic[25,28] properties of pressure-densified polymer glasses. Limited data are available on pressure-densified polystyrene (PS) from a solvent sorption and gas permeation study[23] as well as from thermally stimulated depolarization current (TSDC) measurements.[40] More recently, there have been a number of reports on pressure-densified polymer glasses that have been investigated with quasi-elastic Raman scattering,[42] laser light scattering,[31] small-angle X-ray scattering study of density fluctuation,[33,43,44] and Rayleigh−Brillouin light scattering measurements.[45] The polymers that have been studied most extensively with respect to pressure densification are *a*-PMMA,[13,14,18,21,24,25,27,28,36,38,39,43] *a*-PS,[10,13,14,16,17,19,20,22−25,28−31,33,34,40,41,43−45] PVAc,[11,15,39,43,46,47] and poly(vinyl chloride) (PVC).[25,28,32,35,41] Limited data are available on pressure-densified polycarbonate (PC),[25] poly(cyclohexyl methacrylate) (PCHMA),[26,38] poly(ethylene terephthalate) (PET),[41] substituted styrenes,[20,22,28] phenolphthalein,[12−14,24] colophony,[12,14] and phenolformaldehyde resin.[14] The general effects of pressure on the thermodynamics of T_g on the *PVT*, dielectric, thermodynamic, viscoelastic, and mechanical properties of polymer melts and glasses have been reviewed by O'Reilly,[1] Gee,[48] Ferry,[49] and more recently by Tsirule.[50,51] O'Reilly and, to some extent, Ferry also deal with pressure-densified polymer glasses, whereas McKinney and Simha[52] have more thoroughly reviewed the thermodynamics of the densification process for polymer glasses. A few studies have addressed the technological importance of pressure-densified polymers and their properties with respect to polymer processing.[23,25,53,54] In the literature, there have also been reports on in situ positron annihilation lifetime spectroscopy (PALS) measurements of the pressure dependence of orthopositronium (o-Ps) lifetime τ_3 and intensity I_3 in molecular liquids,[55] polymers,[56−58] and pressurized gas/polymer systems.[59−61] However, to the best of our knowledge, no PALS studies of o-Ps lifetime and intensity in isotropic pressure-densified amorphous polymer glasses have been reported yet.

The aim of this study is to investigate the effect of pressure densification on the macroscopic *PVT* properties versus the microscopic free-volume properties of isotropic atactic PMMA glasses made by cooling from the equilibrium melt under hydrostatic formation pressures up to 200 MPa. The microscopic free-volume properties include the free-volume fraction h, the o-Ps lifetime τ_3, and intensity I_3 as well as the free-volume hole size $V(\tau_3)$. From the statistical thermodynamic Simha−Somcynsky equation-of-state (EOS) theory,[62] we expect relatively large changes in the microscopic volume for changes in the macroscopic volume of about 1.5%. We discuss these results in light of the Simha−Somcynsky EOS theory and the Tait EOS. Furthermore, we correlate the PALS free-volume quantities τ_3 and $V(\tau_3)$ with h determined from the theory that we apply to our own *PVT* data. All *PVT* and PALS studies were made with two sets of thermodynamically and chemically identical PMMA glasses that were isotropic and pressure-densified to yield a large range of densities and free-volume fractions. Thus, we avoid effects associated with differences in molecular weight and thermomechanical history, which ultimately occur when comparing different sets of literature data. We also show and discuss a modified sample cell for a commercial *PVT* apparatus that is suitable for making samples of isotropic pressure-densified polymer glasses for further analysis with PALS and other characterization techniques. During the densification cycle $A \rightarrow B \rightarrow P_0 \rightarrow P_i \rightarrow B_i \rightarrow A_i \rightarrow a_i$ (Figure 1) all samples are subjected to hydrostatic pressure in the sample cell, thus ensuring isotropic pressure-densified glass specimens.

Equations of State and *PVT* Data. We have previously discussed and applied two types of equations of state (EOS) to homopolymer blends in the melt and glassy state:[4] the Tait EOS, which is an empirical description of *PVT* data, and the Simha−Somcynsky EOS, which is based on theoretical considerations. The Tait EOS describes the specific volume v in cm^3/g as a function of pressure P in MPa and temperature T in °C of polymer melts and glasses in terms of a zero-pressure isobar $v(0,T)$, universal constant C of 0.0894[2,63] and the temperature-dependent Tait parameter $B(T)$:

$$v(P,T) = v(0,T)\left\{1 - C \ln\left[1 + \frac{P}{B(T)}\right]\right\} \qquad (1a)$$

where

$$B(T) = B_0 \exp(-B_1 T) \qquad (1b)$$

B_0 and B_1 are constants, and the zero-pressure isobar $v(0,T)$ is described by a first- or higher-order polynomial or exponential expression:

$$v(0,T) = C_0 + C_1 T + C_2 T^2 + C_3 T^3 \qquad (1c)$$

or

$$v(0,T) = v_0 \exp(\alpha_0 T) \qquad (1d)$$

where α_0 is the thermal expansivity evaluated at zero pressure. The lack of a rigorous molecular interpretation of the material-dependent characteristic parameters of the Tait EOS has led to the development and widespread use of EOS theories. One of the most successful EOS theories is the Simha−Somcynsky EOS theory.[2,62,64,65] The theory is based on a quasilattice theory where the molecules, consisting of n chemical repeat units, n-mers, with molecular weight M_r are divided into s equivalent segments, s-mers, with molecular weight M_0 that occupy only a fraction y of the lattice sites. Each chain has $3c$ external, i.e., volume-dependent, degrees of freedom, and the intersegmental potential is based on the 6−12 Lennard-Jones potential in the square-well approximation. The fraction of lattice vacancies, i.e., the statistical mechanical free-volume fraction,[66] is characterized by $h = 1 - y$. Assuming random mixing of vacant and occupied sites of equal size, the number of vacancies disordering the system is determined by the minimization of the Helmholtz free energy for an equilibrium system such as polymer melts. For polymers, contributions from terminal groups become negligible, as s tends to infinity, and the flexibility ratio $3c/s$ is generally assigned the value 1, i.e., one external degree of freedom per segment.[62,66] The Simha−Somcynsky EOS can be written in terms of two coupled equations:[62]

$$\frac{\tilde{P}\tilde{V}}{\tilde{T}} = [1 - 2^{-1/6}y(y\tilde{V})^{-1/3}]^{-1} + \frac{2y}{\tilde{T}}(y\tilde{V})^{-2}[1.011(y\tilde{V})^{-2} - 1.2045] \quad (2a)$$

and

$$\frac{s}{3c}\left[\frac{s-1}{s} + y^{-1}\ln(1-y)\right] = \frac{y}{6\tilde{T}}(y\tilde{V})^{-2}[2.409 - 3.033(y\tilde{V})^{-2}] + \left[2^{-1/6}y(y\tilde{V})^{-1/3} - \frac{1}{3}\right][1 - 2^{-1/6}y(y\tilde{V})^{-1/3}]^{-1} \quad (2b)$$

where $\tilde{P} = P/P^*$, $\tilde{V} = v/V^*$, and $\tilde{T} = T/T^*$ are the reduced PVT variables and $y\tilde{V}$ is the reduced cell volume. P^*, V^*, and T^* are the characteristic scaling parameters in MPa, cm^3/g, and K, respectively, that are determined from PVT equilibrium melt data and contain the molecular characteristics of the system or the structural characteristics of the segment.

In this study, we apply the theory to a homopolymer in the equilibrium melt and in different glassy states effected by pressure densification. In the melt, h can be calculated from eqs 2a and 2b and the scaling parameters P^*, V^*, and T^*. In the glassy state, strictly speaking, eq 2 cannot be applied unconditionally due to violation of the equilibrium assumption. However, assuming P^*, V^*, and T^* to be constant below the pressure-dependent glass transition temperature $T_g(P)$ (Figure 1), the Simha−Somcynsky EOS can also be applied to the glassy state to calculate h.[22,46,47,52,64,67] The latter can be determined using the adjustable parameter (AP) method[22,46] that treats the occupied volume fraction y as an adjustable rather than equilibrium parameter in combination with eq 2a and experimental PVT data. A more consistent but computationally more involved procedure is the partition function (PF) method[47] that makes proper use of the configurational partition function to obtain y from experiment and predicts slightly higher h values and a lower temperature coefficient $\partial h/\partial T$ and pressure coefficient $\partial h/\partial P$, i.e., a less dense but more frozen-in glassy structure than the adjustable parameter method. A first estimate of h values using the PF method can be obtained from Figure 10 in ref 47 using reduced temperatures and pressures. Nevertheless, the numerical differences are usually small,[39,43] as we will show for our PMMA, and therefore the AP method is much more common than the PF method for calculating free-volume fractions in the glassy state.

Positron Annihilation Lifetime Spectroscopy and Free Volume. PALS is a unique analytical technique for studying free volume in polymers.[68−75] PALS involves directly probing the free-volume sites in a polymer by injecting high-energy positrons e^+ (the antiparticle of an electron e^-) that are emitted from a radioactive source such as ^{22}Na together with a 1.28 MeV γ-ray (start-γ). In condensed matter, positrons annihilate in at least three different ways,[76,77] and these annihilation events give rise to characteristic lifetimes. In the first case, the positrons exist as "free" positrons annihilating with an e^- of the medium in 0.3−0.5 ns, whereas in the second and third cases the thermalized positrons can form two metastable bound states with one of the excess e^- in the positron spur. Depending on the relative spin of the two particles, the species thus formed are called parapositronium (p-Ps, spins antiparallel) and orthopositronium (o-Ps, spins parallel). In the Ps, the positron and electron are bound together by 6.8 eV with a mean separation equivalent to the Bohr radius, and thus the size of the Ps is similar to that of the hydrogen atom (Bohr diameter 1.06 Å). In a vacuum, p-Ps and o-Ps annihilate intrinsically after 0.125 and 142 ns, respectively. However, in condensed matter such as polymers, the position of the o-Ps annihilates after localization with a surrounding electron of opposite spin within an o-Ps lifetime τ_3 of 1−5 ns. The latter annihilation is called the pick-off annihilation lifetime. Since τ_3 is inversely proportional to the square of the overlap of the positron component of the Ps wave function with the lattice or cavity wall electron wave function, it is therefore related to the size of the low electron density free-volume sites.[78] Assuming spherical free-volume sites of radius R, obtained by using a spherical potential of radius R_0 with an electron layer of thickness $\Delta R = R_0 - R$, a semiempirical equation between τ_3 in ns, R and R_0 in Å was established[79,80] and optimized with $\Delta R = 1.656$ Å[81] for molecular solids:

$$\tau_3 = \frac{1}{2}\left[1 - \frac{R}{R_0} + \frac{1}{2\pi}\sin\left(\frac{2\pi R}{R_0}\right)\right]^{-1} \quad (3a)$$

$$V(\tau_3) = (4\pi/3)R^3 \quad (3b)$$

In the literature, eq 3 has been widely used for polymers to convert mean τ_3 values to hypothetical radii and volumes of free-volume holes. The distribution of hole sizes has attracted a lot of attention in connection with polymers,[82−90] and one of the more successful computer programs to calculate free-volume distributions in polymers is the maximum entropy lifetime MELT program.[88,89,91,92] The o-Ps formation probability is called o-Ps intensity I_3 and has been claimed to be directly related to the number of free-volume hole sites in polymers. I_3 has found its application in a widespread semiempirical equation for the calculation of free-volume fractions from PALS data:[93]

$$h_{Ps} = CV(\tau_3)I_3 \quad (4)$$

where $V(\tau_3)$ is from eq 3 and C is a constant obtained from a correlation of temperature-dependent PALS data and *PVT* data analyzed in the framework of the Simha−Somcynsky EOS. However, it has also been shown that I_3 is very sensitive to inhibition reactions taking place in the positron spur;[77,94] source exposure time[70,74,95,96] and exposure to visible light,[97] exposure to electric fields,[77,98,99] and magnetic fields.[100] This implies that changes in the o-Ps intensity I_3 cannot be accounted for solely on the basis of free volume.[101]

Experimental Methods

Materials and Sample Preparation. Samples were prepared from atactic poly(methyl methacrylate) (PMMA) (Scientific Polymer Products Inc., Catalog No. 037B) with the following specified properties: $T_g = 105$ °C, $M_w = 75$ kg/mol (GPC, polystyrene standards), density $\rho = 1.20$ g/cm^3, and refractive index $n_{d,20°C} = 1.430$. The PMMA powder was dried at 95 °C for 4 h and slowly cooled to room temperature (RT) under vacuum. Small cylinders (diam 9 × 5 mm), double disks (diam 9.5 × 1.3 + diam 13.5 × 1.7 mm), and disks (diam 13.5 × 3 mm) were then compression-molded between aluminum foil at 185 °C and 200 kN and cooled to RT at approximately 20 °C/min in a Fontijne press TP200. All pressed samples were rejuvenated at 125 °C and atmospheric pressure for 1.5 h, cooled to RT at 0.5 °C/min in dry air, and stored in a desiccator. Mercury and silicone oil 210H (heat-stabilized poly(dimethylsiloxane), Dow Corning) were used as pressure-transmitting fluids for standard *PVT* measurements and pressure densification, respectively.

***PVT* Measurements.** The density of the rejuvenated PMMA samples was measured at 20 °C and 2 atm (helium) with a Micromeritics multivolume pycnometer 1305. The *PVT* properties of all pressure-densified PMMA glasses were measured with a commercial high-pressure bellows-type dilatometer (Gnomix Inc. *PVT* apparatus) using the standard isothermal mode of operation with 5 °C temperature and 10 MPa pressure steps.[3,102] Other modes of operation used to carry out the densification cycles (Figure 1) are isobaric heating at 0.5 °C/min and 10 MPa; isobaric cooling at 0.5 °C/min and densification pressures of 50, 100, 150, and 200 MPa; and data acquisition at RT and 1 MPa after depressurization. The instrument extrapolates data at 0 MPa data from high-pressure data (10−30 MPa, 1 MPa increments) using the Tait EOS. In the context of this paper, 0 MPa implies atmospheric pressure (0.1 MPa), and all elevated pressures are to be interpreted as pressures above atmospheric pressure. The Gnomix *PVT* apparatus is designed to ensure hydrostatic pressure throughout the sample in the melt and semicrystalline as well as the glassy state compared with high-pressure piston-type dilatometers.[3,103] Most of the *PVT* data were analyzed using the evaluation software PVTEVAL (V6.04) from Gnomix Inc. A modified version of the instrument software PVTEX (V6.06) was obtained from Gnomix Inc. and enables the instrument to be run in the data acquisition mode at pressures down to 0 MPa.

Pressure-Densified Samples and Modified *PVT* Apparatus. Our *PVT* data on silicone oil 210H (from 25 to 220 °C and 0 to 200 MPa) lie within 0.5% of the data published by Zoller and Walsh,[3] and we obtain at 25 °C and atmospheric pressure $\kappa = 10.78 \times 10^{-4}$ MPa^{-1} and $\alpha = 9.38 \times 10^{-4}$ °C^{-1}. The corresponding values for mercury used in PVTEX[104] are $\kappa = 0.40 \times 10^{-4}$ MPa^{-1} and $\alpha = 1.80 \times 10^{-4}$ °C^{-1}. Compared with mercury, silicone oil has a much higher compressibility and thermal expansivity and is therefore unsuitable for use as a confining fluid for standard *PVT* measurements in the Gnomix apparatus. This fact precludes simultaneous *PVT* measurements and preparation of pressure-densified samples with silicone oil in the standard *PVT* sample cell of the Gnomix apparatus. For this reason, we have redesigned the sample cell in order to make isotropic disks as well as other geometries of pressure-densified PMMA as shown in Figure 2. The assembly connects with the base and rod carrying the LVDT core of the Gnomix apparatus. The mold consists of three cylindrical parts (3, 4, and 5 in Figure 2) which fit precisely into the cylindrical cavity of the sample chamber (6) that is attached to the long tube (1) by the ring nut (2). The tolerance is such that silicone oil can still flow freely to and from two cylindrical samples (diam 9 × 5 mm) that are initially placed between the mold parts (3, 4, and 5). In the equilibrium melt, the two initially cylindrical samples are shaped into two double disks (black in Figure 2) mainly by the weight of the mold parts (4, 5). The parts' weight-to-height ratio was optimized to give disks with plane parallel surfaces with no overflow at the circumference that could prevent the oil from flowing freely throughout the mold. This was achieved by drilling eight radial holes (diam 2.5 mm, not shown in Figure 2) to the center of each part (3, 4, and 5). Obviously, parts 3 and 5 can be turned upside down to make simple disks as well. Silicone oil can flow freely to and from the sample chamber (6) via the ring nut (2) and three holes in the lock (7). This ensures that the samples are exposed to hydrostatic pressure throughout the densification cycle. The modified sample cell works well with silicone oil, and the densified samples can be easily removed from the mold after depressurization. To remove the silicone oil from the surface of the densified samples, they were washed four times in *n*-hexane. *n*-Hexane, like diethyl ether, is a nonsolvent for PMMA but a solvent for silicone oil.[105] A second set of pressure-densified PMMA samples for PALS measurements was washed four times in diethyl ether. The cleaned samples were stored in a desiccator.

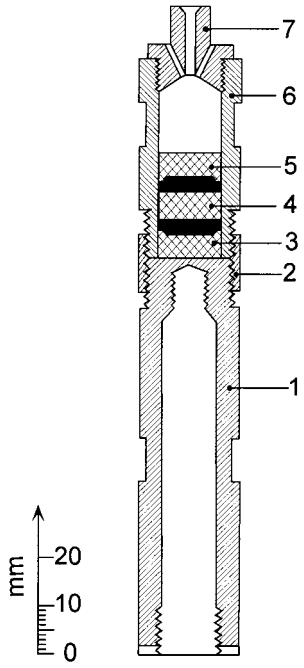

Figure 2. Redesigned sample cell assembly for the Gnomix Inc. *PVT* apparatus to make disks of isotropic densified PMMA glasses. Thread sizes (mm) are given in brackets: 1, long tube (M12 × 1, M4 × 0.7, M18 × 1); 2, ring nut (M18 × 1); 3, 4, 5, sample mold in three parts with two identical samples (black) in between; 6, sample cell (M18 × 1, M14 × 1.25); 7, sample cell lock (M14 × 1.25).

Electron Spectroscopy for Chemical Analysis (ESCA). ESCA (Perkin-Elmer PHI 5500) was used to determine trace elements on the surface of clean, compression-molded PMMA disks before and after washing with *n*-hexane and of disks exposed to silicone oil followed by washing twice and four times with *n*-hexane. The results are summarized in Table 1. The surface of the as-molded and clean PMMA yields the highest ratio of carbon C 1s to oxygen O 1s peaks. This ratio decreases after washing the surface twice with *n*-hexane. Compared with the clean PMMA surface, washed twice with *n*-hexane, we

Table 1. ESCA Results from a Clean, Compression-Molded PMMA Surface and from One Washed Twice in *n*-Hexane and from a PMMA Surface Washed Twice and Four Times with *n*-Hexane after Exposure to Silicone Oil

	clean PMMA		PMMA exposed to silicone oil and	
element[a]	as-molded	washed twice	washed twice	four times
C1	91.26	86.80	68.19	70.03
O1	8.74	13.20	24.51	22.85
Si 2p			4.58	4.84
Cl 2p			1.37	1.00
Na 1s			0.56	0.41
N 1s			0.81	0.86

[a] Concentration in %.

found a small amount of Si and even less of Cl, Na, and N on the sample surface of PMMA that had been washed twice and four times with *n*-hexane after 5 days exposure to silicone oil at RT. All trace elements are evidently from the heat-stabilized silicone oil and its constituents, and washing four times increases the ratio of C1 to O1 by 10% while maintaining the concentration of the trace elements. Since ESCA is a surface-sensitive technique with a penetration depth of approximately 10−100 Å, we consider the residual amounts of trace elements to be negligible in our subsequent PALS measurements, where positron ranges up to 1 mm are common.[76]

Optical Microscopy. The rejuvenated and pressure-densified samples were investigated in an optical microscope (Nikon SMZ-10 and Olympus BH-2) under normal and cross-polarized light. Pictures were taken under these conditions to show the degree of isotropy in the samples.

Positron Annihilation Lifetime Spectroscopy. All PALS measurements were made at RT using a fast−fast coincidence system based on Canberra modules: model 3002 D high-voltage power supply, two 2129 constant fraction differential discriminators, 2058 ns delay, model 2143 time analyzer, 8075 analog-to-digital converter, and a S100 multichannel analyzer board. The two identical γ-ray detectors, placed at approximately 160° to each other and at least 2.5 cm apart to minimize backscattering, consist of CsF crystals mounted on Hamamatsu photomultiplier tubes. The spectrometer has a fwhm of 280 ps, as determined with ^{60}Co, and a channel width of 0.0244 ns, as determined with ^{22}Na. A 2.12 MBq ^{22}Na source, with an active area of approximately diam 1.5 mm, was made by depositing and evaporating a few drops of ^{22}NaCl salt solution on an 8 μm Kapton foil and gluing it with Loctite 406 to an identical piece of Kapton foil. The source gave an effective count rate of approximately 1300 cps when sandwiched between two identical 2−3 mm thick disks, and the assembly was placed equidistant near the center line of the detectors. The PALS measurements were started within 1 h after depressurization in the *PVT* apparatus. Five positron lifetime spectra, each containing 2.5M cts, were collected within approximately 3 h for each sample and evaluated with POSITRONFIT[106] using no source correction and no fixed lifetimes or intensities.

Results

Figure 3a−e shows optical micrographs of our pressure-densified samples under normal (A) and cross-polarized light (B). The absence of birefringence in the plane of the samples implies that they are isotropic and free from residual stresses as opposed to the birefringent compression-molded sample (f). The fact that all samples are isotropic is also evidence for the functionality of our modified sample cell and mold inserts shown in Figure 2.

The specific volume of the glass cooled at 0 MPa (0 MPa glass) as a function of temperature along extrapolated isobars in 50 MPa increments is illustrated in

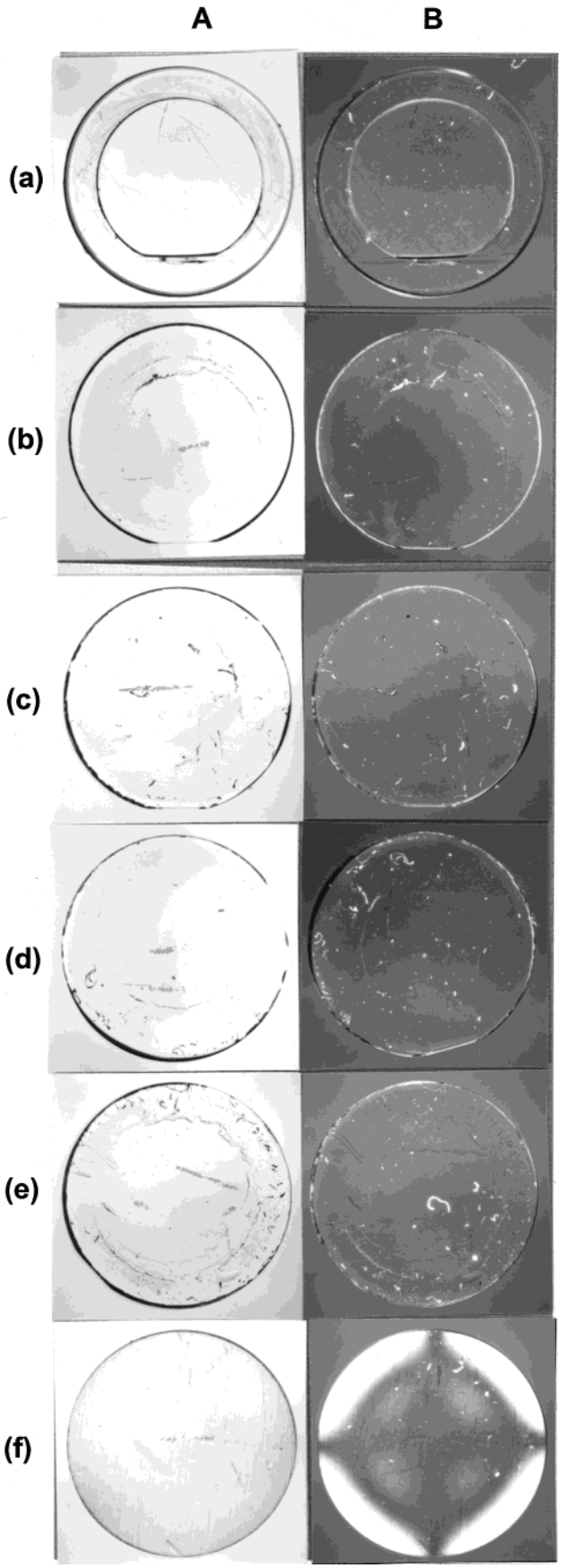

Figure 3. Optical micrographs of PMMA disks (diam 13.5 mm) with different formation histories under normal light (A) and cross-polarized light (B): 0.5 °C/min cooling rate and P_d (a) 0 MPa, (b) 50 MPa, (c) 100 MPa, (d) 150 MPa, (e) 200 MPa, and (f) compression molded.

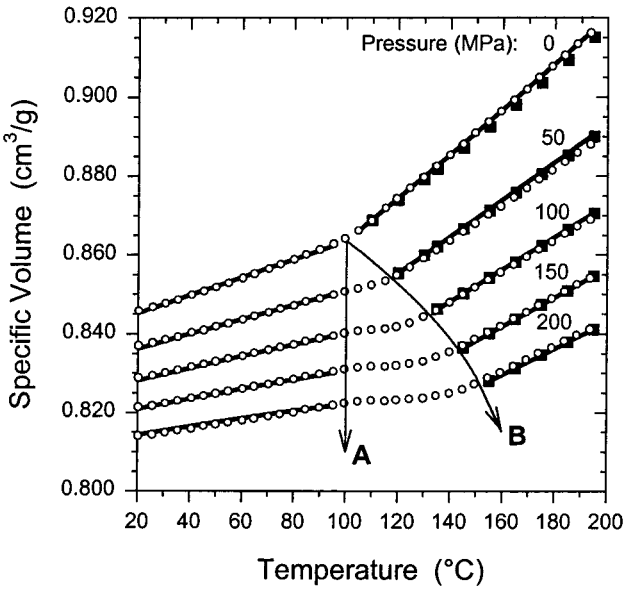

Figure 4. Specific volume of a 0 MPa glass of PMMA, shown as a selection of extrapolated isobars versus temperature: experimental data (○); Tait EOS (—); Simha−Somcynsky EOS (■). Lines A and B represent the zero-pressure glass transition temperature $T^*_g(0,0)$ and the glass transition temperature as a function of pressure $T^*_g(P,0)$, respectively.

Table 2. Simha−Somcynsky EOS Characteristic Scaling Parameters (Eqs 2a,b) for Pressure-Densified PMMA Glasses

densification press. (MPa)	T range[a] (°C)	dev[b] (%)	P^* (MPa)	V^* (cm³/g)	T^* (K)
0	105−194	91.9/6.7/1.4	1076.5	0.8300	11319.7
50	115−194	91.3/7.6/1.1	1076.0	0.8306	11340.1
100	114−193	91.3/7.6/1.1	1076.4	0.8309	11359.9
150	115−194	91.3/7.6/1.1	1061.6	0.8324	11443.8
200	115−194	92.0/6.5/1.5	1070.1	0.8314	11389.3
mean value			1072.1	0.8311	11389.3
std dev			± 6.5	± 0.0009	± 48.3
% std dev			(0.61%)	(0.12%)	(0.43%)

[a] $T_g(P,P_d)$ from eq 5a taken into account. [b] First figure, 0−0.001 cm³/g range; second figure, 0.001−0.002 cm³/g range; third figure, 0.002−0.003 cm³/g range.

Figure 4. The *PVT* data were measured isothermally, and it is common to show the data as a series of extrapolated isobars. The experimental *PVT* data are well described by the Simha−Somcynsky EOS in the equilibrium melt above the pressure-dependent glass transition temperature $T^*_g(P,0)$, and the characteristic scaling parameters P^*, V^*, and T^* of eq 2 are given in Table 2. The Tait EOS reproduces the experimental data well in both the melt and the glassy state below $T^*_g(0,0)$, and the relevant parameters of eq 1 are shown in Table 3 and Table 4, repectively. $T^*_g(P,0)$ (line B) is created by the intersection of the quasi-equilibrium extrapolated isobars lying to the left of line A and those from the equilibrium melt lying to the right of line B. The points of intersection can be fitted to two second-order polynomials:

$$T^*_g(P,P_d) = T^*_g(0,P_d) + a_1P - a_2P^2 \qquad (5a)$$

$$v^*_g(P,P_d) = v^*_g(0,P_d) - b_1P + b_2P^2 \qquad (5b)$$

whose coefficients are given in Table 5 for all pressure-densified glasses. Between lines A and B a glass is re-

Table 3. Tait EOS Parameters (Eqs 1a−d) in the Glassy State of Pressure-Densified PMMA Glasses

Tait EOS parameters	densification pressure P_d (MPa) 0	50	100	150	200
T range (°C)	20−95	20−70	20−65	20−60	20−55
deviation[a] (%)	100/0	100/0	100/0	100/0	100/0
B_0 (MPa)	429.6	440.7	464.0	471.4	477.4
$B_1 \times 10^3$ (°C^{-1})	4.164	3.530	3.849	3.884	3.992
C_0	0.8422	0.8402	0.8373	0.8360	0.8338
$C_1 \times 10^5$	16.4610	16.6340	12.8100	6.7430	5.5696
$C_2 \times 10^6$	0.55275	0.44449	1.0591	1.9120	2.3570
v_0 (cm³/g)	0.8407	0.8394	0.8356	0.8333	0.8308
$\alpha_0 \times 10^4$ (°C^{-1})	2.6750	2.4300	2.581	2.6210	2.7770

[a] First figure, 0−0.001 cm³/g range; second figure, 0.001−0.002 cm³/g range.

Table 4. Tait EOS Parameters (Eqs 1a−d) in the Melt State of Pressure-Densified PMMA Glasses

Tait EOS parameters (eqs 1a−d)	densification pressure P_d (MPa) 0	50	100	150	200
T range[a] (°C)	110−194	120−194	119−193	119−194	119−194
deviation[b] (%)	74.0/26.0	73.5/26.5	72.8/27.2	73.2/26.8	72.8/27.2
B_0 (MPa)	300.6	285.9	287.9	289.4	288.2
$B_1 \times 10^3$ (°C^{-1})	4.257	3.947	3.967	4.005	3.982
C_0	0.8065	0.8059	0.8061	0.8066	0.8062
$C_1 \times 10^4$	5.6572	5.7031	5.6870	5.6498	5.6765
v_0 (cm³/g)	0.8105	0.8103	0.8107	0.8111	0.8108
$\alpha_0 \times 10^4$ (°C^{-1})	6.3340	6.3590	6.3280	6.2890	6.3110

[a] $T_g(P,P_d)$ from eq 5a taken into account. [b] First figure, 0−0.001 cm³/g range; second figure, 0.001−0.002 cm³/g range.

Table 5. Glass Transition Functions (Eqs 5 and 6) for Extrapolated Isobars and Cooling Isobars

glass transition functions	densification pressure P_d (MPa) 0	50	100	150	200
extrapolated IB[a]					
T range (°C)	20−95	20−70	20−65	20−60	20−55
$T^*_g(0,P_d)$ (°C)	100.5	90.9	82.5	76.2	72.3
a_1	0.3769	0.3667	0.3315	0.2701	0.2813
$a_2 \times 10^4$	6.2225	3.6831	1.2344	−1.8732	−1.5555
$v^*_g(0,P_d)$ (cm³/g)	0.8634	0.8579	0.8534	0.8499	0.8476
$b_1 \times 10^4$	1.9259	1.6401	1.6194	1.6672	1.5719
$b_2 \times 10^7$	0.7488	0.5937	1.2619	1.8963	1.7262
at $P = P_d$					
$T^*_g(P,P_d)$ (°C)	101.1	108.3	114.2	120.6	136.4
$v^*_g(P,P_d)$ (cm³/g)	0.8636	0.8497	0.8384	0.8292	0.8233
cooling IB[a] ($P = P_d$)					
$T_g(P)$ (°C)	101.1	110.4	118.6	128.3	138.5
$v_g(P)$ (cm³/g)	0.8637	0.8505	0.8388	0.8301	0.8220

[a] IB = isobar.

formed by pressurizing from the melt during isothermal compression (cf. path b→b_i→B_i→A_i→a_i in Figure 1). This glass does not possess the same physical properties as that originally loaded into the *PVT* apparatus, and it is different for each isotherm in the "wedge" between lines A and B. The pressure-densified glasses thus produced have a lower specific volume than the glass that was originally loaded into the *PVT* apparatus. Hence, the "valleys" along the extrapolated isobars between lines A and B. Unlike the commercial-grade PMMA used in our previous *PVT* study on polymer blends,[4] the PMMA used in this work does not contain any copolymer, and our *PVT* data for the research-grade PMMA are in very good agreement with those reported in the literature.[3,8,26,38,67, 107−112]

In Figure 5, the experimental *PVT* surface of the 0 MPa glass from Figure 4 is shown together with that of the glass that was pressure-densified at 200 MPa (200 MPa glass). The salient features are the two glass

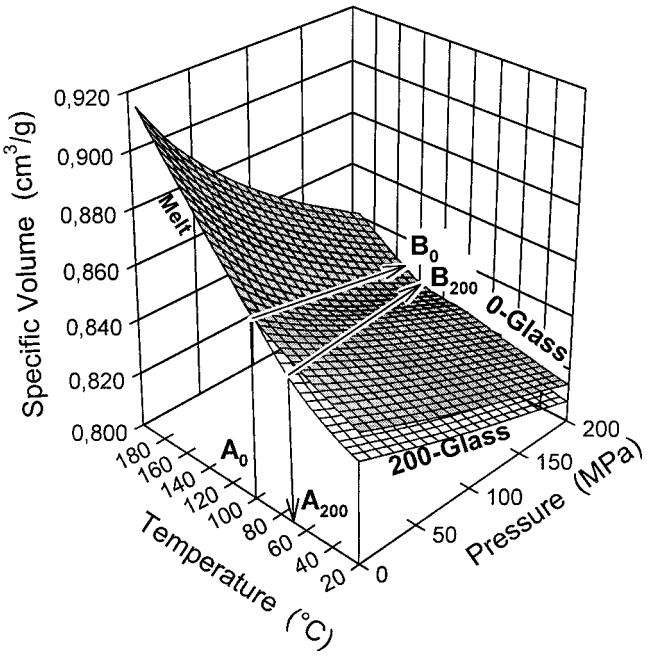

Figure 5. Experimental *PVT* surfaces of PMMA glasses: 0 MPa glass (gray mesh) and 200 MPa glass (open mesh). Each mesh point represents an experimental data point. A_0 and A_{200} are the glass transition temperatures for the two glasses at zero pressure, respectively, and B_0 and B_{200} are their pressure-dependent and formation-pressure dependent $T^*_g(P,P_d)$.

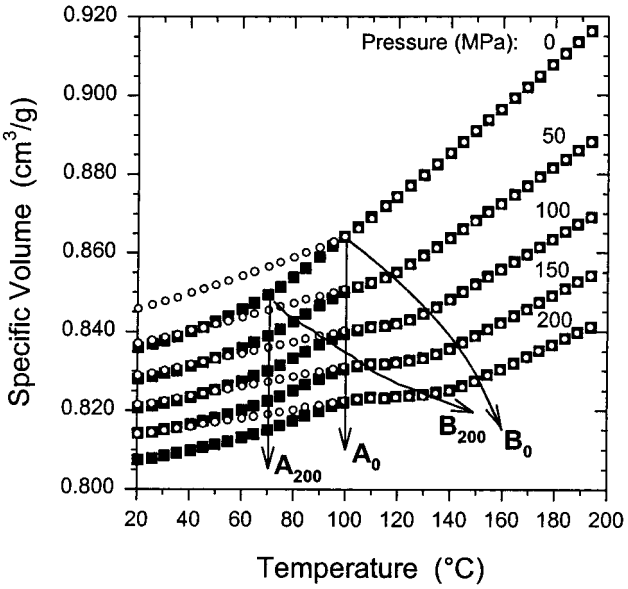

Figure 6. Extrapolated isobars of the 0 MPa glass (○) and 200 MPa glass (■) in 50 MPa increments versus temperature; data from Figure 5. Volume relaxation of the 200 MPa glass is evident above approximately 55 °C. The specific volume of the 200 MPa glass has returned completely to the equilibrium melt state above approximately 100 °C.

surfaces that are distinctly displaced from each other by an amount equal to the decrease in specific volume due to pressure densification; the 200 MPa glass returns completely to the equilibrium melt around 100 °C such that the melt *PVT* surfaces of both glasses coincide within experimental error; the glass transition of the 200 MPa glass occurs near 70 °C, i.e., approximately 30 °C below $T^*_g(0,0)$; and volume relaxation occurs well below $T^*_g(0,200)$, as evidenced by the two merging glass surfaces (below line A_{200}). The observed depression of T_g with P_d and the volume relaxation below T_g are in good agreement with previous reports on pressure-densified PMMA[13,21,24,28] as well as PS[10,13,23,24,28,29,40] and PVAc.[11] The features observed in Figure 5 are emphasized in Figure 6 with extrapolated isobars in 50 MPa increments. The onset of volume relaxation in the 200 MPa glass starts around 55 °C during isothermal compression with an effective heating rate of 0.3 °C/min, as seen by the merging extrapolated isobars of the two glasses. $T^*_g(P,200)$ (line B_{200}) is obtained similar to $T^*_g(P,0)$ (line A_0), but the intersection of the pressure-densified glassy *PVT* surface with the melt surface is more difficult to determine accurately because of the reduced temperature range of the glassy *PVT* surface as a result of volume relaxation. For example, the point of intersection at 200 MPa of the 200 MPa glass requires an extrapolation of the data in the glassy state (20−55 °C) from 55 to 130 °C, and the error can be significant. In fact, it can be shown that a 5 °C change in the temperature range of the glass *PVT* data changes the temperature of intersection by about 3 °C. The Tait EOS parameters of the 200 MPa glass in Table 3 suggest a very good fit of the limited *PVT* surface in the glassy state. In the equilibrium melt, both the Tait EOS and the Simha−Somcynsky EOS are expected to give parameters very similar to those obtained for the 0 MPa glass because volume relaxation of the densified glass is essentially complete above $T^*_g(0,0)$, as shown in Figures 5 and 6. The Tait EOS parameters and Simha−Somcynsky EOS characteristic scaling parameters of the two glasses are indeed identical within experimental error, as shown in Tables 4 and 2, respectively. Similar observations can be made in Tables 2−4 for the *PVT* surfaces in the glassy state and in the equilibrium melt of the pressure-densified glasses that were formed at 50, 100, and 150 MPa.

In Table 3, the thermal expansivity of the pressure-densified glasses lies between 2.43 and 2.77 × 10^{-4} °C^{-1} but does not vary systematically. McKinney and Goldstein[11] have reported a slightly increasing α_0 with increasing formation pressure of their two PVAc glasses, whereas Vleeshouwers and Nies[54] have predicted a decrease in α_0 for the same PVAc glasses. Naoki et al.[32] have found that α_0 of their PVC glasses is nearly constant up to formation pressures of 300 MPa followed by a decrease at 500 MPa. Using eq 1 and data from Table 3, it can be shown that the isothermal compressibility of our PMMA glasses decreases by up to 10.3% with increasing P_d. This compares well to a 2.7% decrease in isothermal compressibility of the 80 MPa PVAc glass.[11] On the other hand, the predicted increase in isothermal compressibility of the same glass by Vleeshouwers and Nies[54] cannot be explained and must be an artifact of their simulation. Our results are also in good agreement with those of the PVC glasses[32] whose compressibility decreased by up to 6%.

The isobars used to make the pressure-densified glasses at a cooling rate of 0.5 °C/min are shown in Figure 7 together with the zero-pressure extrapolated isobar of the 0 MPa glass. The different formation pressures give rise to a pressure-dependent glass transition temperature $T_g(P)$ and volume $v_g(P)$ (line B):

$$T_g(P) = 101.3 + 0.166P + 9.651 \times 10^{-5}P^2 \quad (6a)$$

$$v_g(P) = 0.8635 - 2.823 \times 10^{-4}P + 3.773 \times 10^{-7}P^2 \quad (6b)$$

where T_g, v_g, and P are in °C, cm³/g, and MPa,

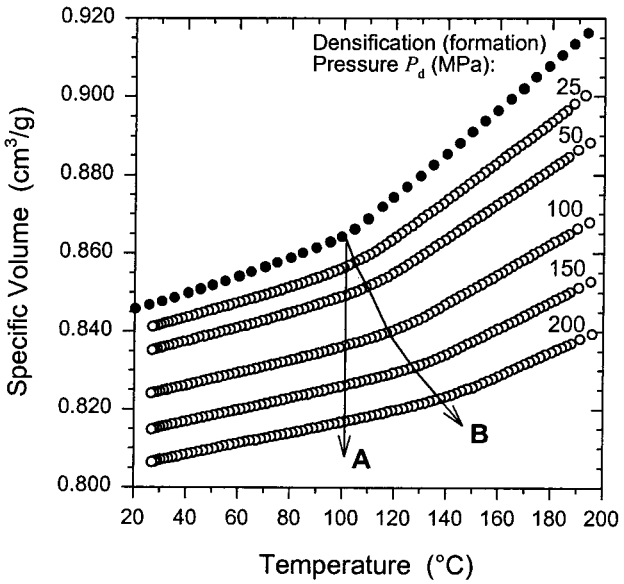

Figure 7. Specific volume of PMMA versus temperature at the formation pressures shown and a cooling rate of 0.5 °C/min (○); zero-pressure *PVT* data (●) from Figure 4. Each variable formation history glass was depressurized at RT to give pressure-densified glass samples for subsequent PALS studies.

respectively. Line A corresponds to $T_g(0)$. No PALS samples with $P_d = 25$ MPa were made, and the *PVT* data are restricted to the cooling isobar. Each isobar generates its own *PVT* surface in the glassy state when the pressure is released at 20 °C, and the glass is compressed isothermally, as illustrated in Figures 1 and 5. The glass transition temperature $T^*_g(P,P_d)$ (eq 5a) and glass transition volume $v^*_g(P,P_d)$ (eq 5b) of each glass are obtained from its line of intersection with the equilibrium melt surface and must be the same as $T_g(P)$ (eq 6a) and $v_g(P)$ (eq 6b) from the cooling isobars when P is equal to the formation pressure P_d. Table 5 shows that $T^*_g(P_d,P_d) = T_g(P_d)$ and $v^*_g(P_d,P_d) = v_g(P_d)$ are indeed satisfied within experimental error (±3 °C and ±0.002 cm³/g) for all P_d except for 150 MPa where the temperature deviation is 8 °C. Similar experimental errors of about ±3 °C have been reported for PVAc.[11] Moreover, the first Ehrenfest relation $dT^*_g/dP = \Delta\kappa/\Delta\alpha$, where $\Delta\kappa$ and $\Delta\alpha$ are the difference in isothermal compressibility and thermal expansivity at T^*_g, derives from thermodynamics[16] and must hold true tautologically[9] within experimental error if the left- and right-hand side are evaluated from the same set of *PVT* surfaces. Both the 0 MPa glass and the 100 MPa glass give an excellent agreement between the pressure coefficient of T^*_g and $\Delta\kappa/\Delta\alpha$, considering the fact that experimental errors of 15% are not unusual.[4] In this respect, the agreement of dT^*_g/dP and $\Delta\kappa/\Delta\alpha$ of the 200 MPa glass within 23% can still be considered satisfactory. Our data in Table 6 also show that the Simha−Boyer relation,[113] $\Delta\alpha_0 T_g \sim$ constant, fails even at densification pressures above 80 MPa.[46] Previously, it has been shown that this relation fails for low- and high-pressure glasses as a function of applied pressure.[20] In this context we can also add Bauwens' conclusion[114] that T_g is related to a constant fraction (~0.118) of activated segments and not to a constant fraction of free volume, as implied by Simha−Boyer's iso-free-volume relation. It is known that $dT_g/dP < \Delta\kappa/\Delta\alpha$, which is perhaps not so surprising in view of the fact that dT_g/dP is evaluated from *PVT* surfaces of variable formation history glasses

Table 6. Glass Transition Parameters of Pressure-Densified PMMA Glasses

	PMMA		
eqs 7 and 10	0 MPa	100 MPa	200 MPa
$T^*_g(0,P_d)$ (°C)	100.5	82.5	72.3
$dT^*_g/dP(0,P_d)$ (°C/MPa)	0.377	0.332	0.281
$\alpha_g \times 10^4$ (°C^{-1})	2.675	2.581	2.777
$\alpha_l \times 10^4$ (°C^{-1})	6.334	6.328	6.311
$\Delta\alpha_0 \times 10^4$ (°C^{-1})	3.659	3.747	3.534
$\kappa_g \times 10^4$ (MPa^{-1})	3.149	2.642	2.4999
$\kappa_l \times 10^4$ (MPa^{-1})	4.543	3.853[b]	3.722[c]
$\Delta\kappa_0 \times 10^4$ (MPa^{-1})	1.394	1.211[b]	1.223[c]
$\Delta\kappa_0/\Delta\alpha_0$ (°C/MPa)	0.381	0.323[b]	0.346[c]
$\Delta\alpha_0 \times T_g$	0.137	0.133	0.122
$(\delta h/\delta T)^a_g \times 10^4$ (°C^{-1})	1.628	1.599	1.580
$(\delta h/\delta T)^a_m \times 10^4$ (°C^{-1})	5.466	5.458	5.415
$F_T(0,P_d)$	0.702	0.707	0.708

[a] Calculated from experimental *PVT* data using *P**, *V**, and *T** for the 0 MPa glass. [b] Calculated from low-pressure *PVT* data at 82.5 °C. [c] Calculated from low-pressure *PVT* data at 72.3 °C.

whereas $\Delta\kappa/\Delta\alpha$ is calculated from constant formation history *PVT* data. If the order parameter h is invoked, the two quantities can be reconciled in a modified Ehrenfest relation:[22,46]

$$dT/dP = \Delta\alpha/\Delta\kappa + (\partial T/\partial h)_P(dh/dP) \qquad (7)$$

where the first h-derivative is calculated in the equilibrium melt (eq 2) and the second h-derivative is determined along $T_g(P)$. From our PVT data in Tables 5, 6, and 2 we have evaluated eq 7 for the 0 MPa glass and find $0.166 = 0.381 + (5.466 \times 10^{-4})^{-1} \times (-1.320 \times 10^{-4})$, which approximates to 0.17↔0.14 and is quite good considering the 15% uncertainty mentioned above. For the pressure-densified glasses, $\Delta\kappa/\Delta\alpha$ becomes difficult to evaluate due to the volume relaxation in the transition region of the *PVT* diagrams, and consequently, the errors involved in eq 7 increase substantially.

The specific volume v and density ρ of the pressure-densified glasses as a function of the densification pressure P_d at 20 °C and 1 atm are shown in Figure 8a, and obviously v and ρ decrease and increase linearly with increasing P_d, respectively. The densification, $D = (\rho_{Pd} - \rho_0)/\rho_0$, in Figure 8b also increases linearly with increasing P_d up to a maximum value of 1.2% at 200 MPa, which is consistent with the densifications reported for PMMA at an equivalent P_d of 200 MPa by Shishkin (1.5%),[14] Kimmel and Uhlmann (0.8−1.4% for high-low molecular weight),[18] Bree et al. (approximately 1.2%),[25] Wetton and Moneypenny (approximately 1.4%),[28] and Price (1.26%).[27] All these values are only a fraction of the maximum densification possible for PMMA. To achieve high densifications, the equilibrium melt has to be pressurized to high formation pressures. The pressure dependence of T_g implies, however, that high pressures can be applied at only high temperatures where thermal degradation may occur. Since the pressure coefficient of the degradation temperature T_d is about 1 order of magnitude smaller than that of T_g, there will be a temperature and pressure above which the polymer will either thermally degrade or enter the glassy state. This pressure is the maximum P_d that can be applied, thus defining the maximum densification D_{max} that can be achieved in polymer glasses:[52]

$$D_{max} = \kappa' P_{d,max} \qquad (8)$$

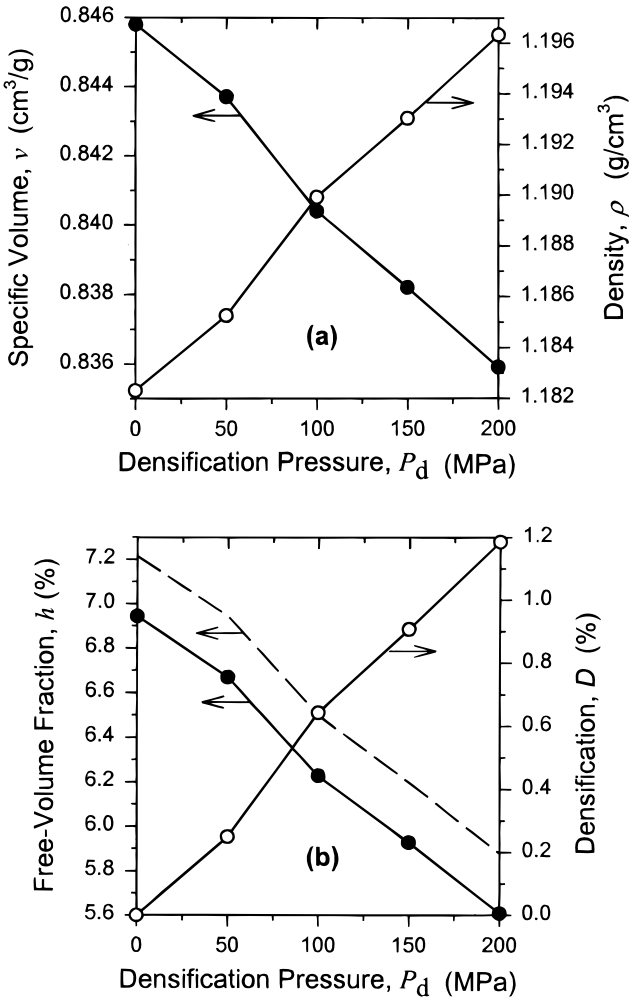

Figure 8. (a) Specific volume v (●) and density ρ (○) of pressure-densified PMMA glasses versus densification pressure P_d at 20 °C and 1 atm. (b) Free-volume fraction h from the adjustable parameter method (●) and from the partition function method (- - -) and densification $D = (\rho_{Pd} - \rho_0)/\rho_0$ (○) versus P_d. Lines are guidelines.

where the densification rate $\kappa' = -(\partial v/\partial P_d)/v$ and $P_{d,max} = [T_d - T_g(0)]/(dT_g/dP)$. From eq 8 and data from Figure 8a as well as a dT_g/dP of 0.187 °C/MPa averaged over 0−200 MPa (Table 5), we obtain 5.7% for our PMMA. This is in excellent agreement with McKinney and Simha's estimate of 5% for *a*-PMMA based on a T_d of 279 °C from pyrolysis data.[52] Shishkin[14] extrapolated the equilibrium melt isobar below T_g in order to estimate D_{max} at the depressurization temperature T_{dp} from the difference in thermal expansivity in the melt and the glass:

$$D_{max} = (\alpha_m - \alpha_g)(T_g - T_{dp}) \qquad (9)$$

Together with our data from Tables 3−5, this approach yields 2.9% for PMMA and is lower than the value estimated from eq 8 but agrees well with the 2% estimated for PMMA by Shishkin.[14]

The free-volume fraction h in Figure 8b decreases with increasing P_d . h was calculated from the Simha−Somcynsky theory and the characteristic scaling parameters for the 0 MPa glass (Table 2) using the AP method (filled circles) as well as the PF method (dashed line) explained in the Introduction. Replacing the characteristic scaling parameters for the 0 MPa glass with the mean values given in Table 2 would reduce all h values by about 2%. The h values obtained from the more rigorous PF method are systematically about 4% larger than those calculated with the AP method. Similar results have been reported by Simha and coworkers.[39,43] We consider that the AP method gives sufficiently accurate h values because the differences between the two methods are small compared with the changes in h caused by pressure densification.

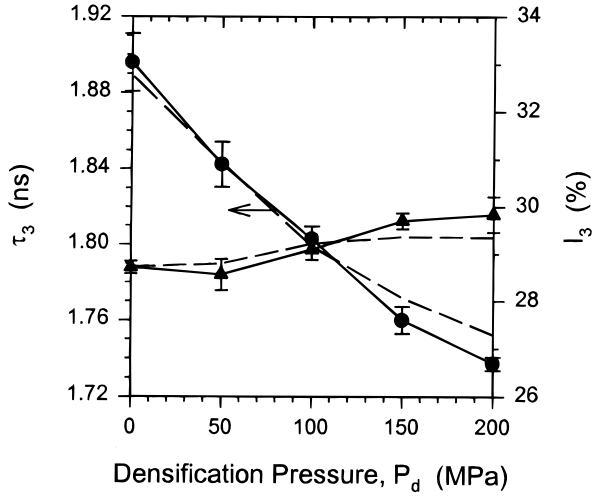

Figure 9. o-Ps lifetime τ_3 (●) and o-Ps intensity I_3 (▲) versus P_d: symbols are for samples washed in *n*-hexane; dashed lines are average values from these samples together with samples washed in diethyl ether. Lines are guidelines.

The o-Ps lifetime τ_3 and o-Ps intensity I_3 of our pressure-densified glasses as a function of P_d at 20 °C and 1 atm can be seen in Figure 9. The symbols represent a set of samples that was washed in *n*-hexane to remove silicone oil from the samples' surface, and every point is an average of five PALS spectra, each containing 2.5M counts. τ_3 decreases substantially with P_d, whereas I_3 remains relatively constant with an average value of 29 ± 0.5%. The dashed lines are average values from these samples together with a second set of samples that was washed in diethyl ether. The results thus obtained show that our data are reproducible within experimental errors that lie well within those found in an international interlaboratory comparison of positron and positronium lifetimes in polymers[115] and that both solvents efficiently remove silicone oil from the surface of the samples and do not affect the results.

Discussion

One of the prerequisites of this study is the preparation of isotropic pressure-densified PMMA glasses. Anisotropy can affect both macroscopic and microscopic volume measurements. In Figure 3, we show that all of our samples are free from birefringence. Therefore, we can conclude that all our glasses are isotropic and that our modified sample cell illustrated in Figure 2 is working properly.

When dealing with pressure-densified polymer glasses, the fact has to be considered that their volume is not in a state of equilibrium.[10,21,23,24,29] The metastable volume of pressure-densified glasses relaxes well below the glass transition temperature of a corresponding glass formed by cooling from the equilibrium melt at atmospheric pressure, as shown in Figures 5 and 6. The volume of the 200 MPa glass starts to relax already at about 55

°C, i.e., 30 °C below T_g*(0,0), during a series of isothermal compressions with an effective heating rate of 0.3 °C/min. Therefore, we have measured the time dependence of the volume of all pressure-densified PMMA samples at 1 MPa—measurements at 0 MPa are possible for only about 30 min with the Gnomix apparatus—and RT over a period of 5 h and found no volume relaxation during that time. Since all our PALS measurements were made within 5 h of depressurization, we conclude that our PALS samples are not affected by volume relaxation.

The main objective of this study is to investigate the effect of pressure densification on the macroscopic *PVT* properties versus the microscopic volume properties of a series of chemically identical PMMA glasses differing only in density, as a result of different formation pressures during cooling from the equilibrium melt. As we have shown in Figure 8a, the macroscopic volume decreases linearly with increasing densification pressure, and the densifications thus obtained (Figure 8b) agree very well with those in the literature. Likewise, the microscopic volume represented by the free-volume fraction (Figure 8b) that is calculated from our *PVT* data and the Simha–Somcynsky theory decreases linearly but more substantially than v with increasing P_d. The average microscopic volume size, represented by the o-Ps lifetime τ_3, also decreases significantly with P_d , as we have shown in Figure 9. Some deviation from linearity occurs at high formation pressures. The o-Ps intensity I_3 , on the other hand, is constant and independent of P_d within experimental error, i.e., 29 ± 0.5%. This is an expected result because changing the physical structure of a polymer should not affect chemical reactions in the positron spur, such as ionization, recombination, anion formation, and positron capture, which all can contribute to a quenching of positrons and an inhibition of positronium formation, i.e., a reduced o-Ps intensity I_3. In contrast to our result, Wang et al.[57] have reported an in situ high-pressure PALS study of amine-cured epoxy polymers, where I_3 is pressure-dependent such that it decreases nonlinearly from 24% at 0 MPa to about 22.5% at 200 MPa in the melt. Similarly, in the glassy state at RT, where Wang et al.'s samples are anisotropic and the PALS data become path-dependent, I_3 decreases from 24.5% at 0 MPa to about 23% at 200 MPa. On the other hand, their nonlinear decrease of τ_3 with increasing pressure in both the melt and the glassy state is in agreement with our results. It is also noteworthy that a constant o-Ps intensity I_3 has also been observed in a combined uniaxial tensile and PALS study of PMMA,[116] where the o-Ps lifetime τ_3 was shown to increase by up to about 3%. Similarly, in another uniaxial tensile and PALS study of PC,[117] I_3 was constant whereas τ_3 and the specific volume increased by up to 3% and 0.6%, respectively. Ruan et al.[117] calculated a 5% increase in free-volume fraction from their PALS data according to eq 4, which happens to be also the fractional change in the equivalent spherical cavity volume $V(\tau_3)$ (see eq 3b) because of the constant I_3 values.

In PALS studies of polymers, the change in τ_3 in Figure 9 (0.16 ns) that is induced by physical structural changes is rather large and can otherwise only be achieved by significant changes in the chemical structure of polymers. However, such chemical structural changes often imply changing the positron and positronium chemistry, too, and hence I_3.[75,89,94] Together with

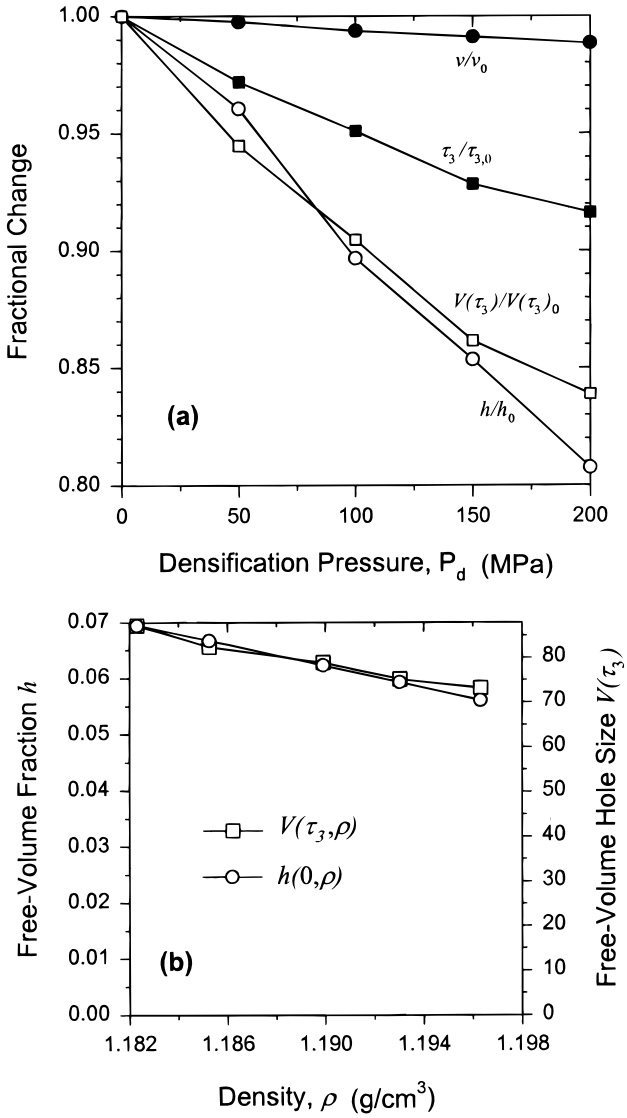

Figure 10. (a) Fractional change in specific volume v (●), free-volume fraction h (○), o-Ps lifetime τ_3 (■), and free-volume hole size $V(\tau_3)$ (□) at 20 °C and 1 atm versus P_d; $V(\tau_3)_0 = 87.2$ Å^3. (b) h and $V(\tau_3)$ versus ρ. Lines are guidelines.

the fact that I_3 is independent of P_d , we have strong experimental evidence to suggest that any change in the microscopic volume due to changes in the macroscopic volume can only be explained in terms of the average free-volume cavity size that is linked to τ_3 via the semiempirical eq 3a. To establish any correlation between the macroscopic and microcopic volume parameters of the pressure-densified glasses, we have calculated equivalent spherical hole volumes $V(\tau_3)$ from our τ_3 data in Figure 9 and eq 3a. In a normalized representation we show the fractional changes of the specific volume, o-Ps lifetime τ_3, equivalent spherical hole volume $V(\tau_3)$ (eq 3b), and free-volume fraction h at RT and atmospheric pressure versus densification pressure P_d in Figure 10a. All parameters are normalized with respect to the values of the 0 MPa glass and $V(\tau_3)_0 = 87.2$ Å. The pertinent features are that a comparatively small change of 1.2% in the macroscopic volume yields significant changes in the microscopic volume, as seen in the free-volume quantities τ_3 (8.4%), $V(\tau_3)$ (16.1%), and h (19.2%). Moreover, h from the Simha–Somcynsky theory and *PVT* data correlates better with $V(\tau_3)$ than with τ_3 from PALS, despite the fact that the underlying

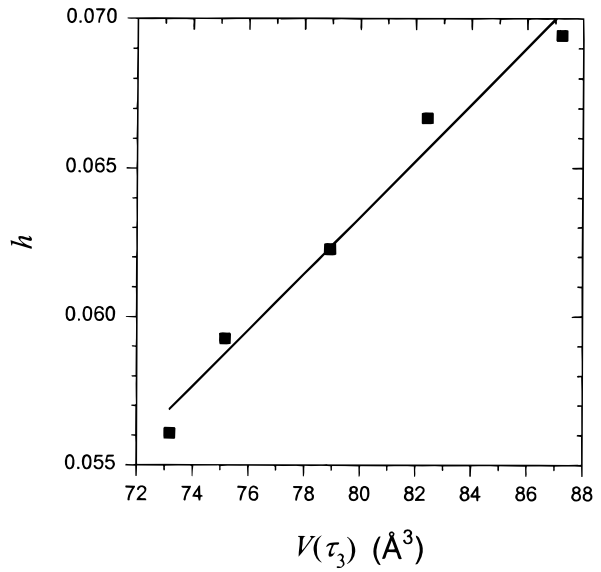

Figure 11. h versus $V(\tau_3)$. First-order linear regression line: $h = -0.01245 + 9.474 \times 10^{-4}V(\tau_3)$ ($r^2 = 0.9778$).

conversion of τ_3 values to equivalent hole radii is at best semiempirical for polymers and assumes hypothetical spherical free-volume hole sites. A plot of h and $V(\tau_3)$ versus ρ is shown in Figure 10b and emphasizes the correlation of h with $V(\tau_3)$. Consequently, we have further investigated h as a function of $V(\tau_3)$, and in Figure 11 the two free-volume quantities are seen to correlate linearly. It is interesting to note that, if the linear correlation is extrapolated to a hypothetical free-volume fraction of zero, one obtains an equivalent hole radius $R(\tau_3)$ that is close to 1.4 Å (1.46 and 1.35 Å for the AP and PF method, respectively) which compares to the Bohr diameter (1.06 Å) of the o-Ps species. Although the extrapolation has to be treated with great care, because of the lack of data in the h range of 0.056−0, it nevertheless suggests the need to further investigate whether it is possible to approach the smallest free-volume cavity size that can still be measured by the o-Ps species by applying sufficiently large densification pressures, albeit difficult to achieve experimentally. Alternatively, the result suggests the need to investigate whether τ_3 levels off at sufficiently high densification pressures, as is observed for τ_3 at cryogenic temperatures in low-temperature PALS measurements. Incidentally, in a separate temperature-dependent PALS study[101] of a 0 MPa PMMA glass, we found, at our lowest measuring temperature of 80 K, a value of τ_3 of 1.66 ns or $R(\tau_3)$ of 2.5 Å. A similar value of τ_3 at 80 K was reported by Wang et al.[74] for another grade of PMMA.

Despite the good correlation of h with $V(\tau_3)$, the fact cannot be neglected that the glassy structure of polymers depends not only on the free-volume fraction but also on how much the free volume is frozen-in below T_g relative to the melt. This second-order parameter has been defined as a freezing fraction[38,46,67] F_T that is a measure of the variation of the free-volume fraction h with temperature in the glassy state relative to that in the equilibrium melt:

$$F_T = 1 - [(\partial h/\partial T)_g/(\partial h/\partial T)_m] \qquad (10)$$

A freezing fraction of one corresponds to a completely frozen glass, i.e., a glass with a constant free-volume fraction. A liquidlike glass, on the other hand, would behave like the equilibrium melt and is thus assigned a F_T value of zero. High-T_g polymers tend to have freezing fractions near 0.5, whereas low-T_g polymers lie closer to one.[67] In Table 6 we show freezing fractions for three of our pressure-densified glasses that were all evaluated at atmospheric pressure. Evidently, within two decimals F_T does not depend on the formation pressure in the range 0−200 MPa. In other words, the application of formation pressures up to 200 MPa does not produce glassy structures that are more frozen-in and thus closer to equilibrium than nondensified glasses, which contradicts Shishkin's assumption.[14] A similar result was obtained by McKinney and Simha[46] for their PVAc glasses, but only up to a formation pressure of 80 MPa. They interpreted the apparent invariance of F_T with P_d as being consistent with the hypothesis of a single entropy surface proposed by Goldstein.[9] The constant freezing fractions could explain Bree et al.'s[25] observation that, in contrast to physical aging, the much larger volume changes due to pressure densification have almost no effect on the mechanical relaxation times and the creep rate of PVC. In a recent quasi-elastic Raman scattering study[42] we have shown that the refractive index of our pressure-densified PMMA glasses increases with density according to the Lorentz−Lorenz equation, as has also been shown for physically aged PS.[118] In this context it is worth mentioning that the rate of change in refractive index with density of the latter is about 0.4 cm^3/g, which is almost the same as that of the former (0.37 cm^3/g).

McKinney and Goldstein's reasoning[11] supports Bree et al.'s finding[25] on mechanical relaxation times that longer relaxation times are produced by slow cooling rather than pressure densification because of the apparent dominance of entropy over volume in determining relaxation times. Further evidence in support of formation path-dependent properties of polymer glasses was given by Weitz and Wunderlich,[24] whose enthalpy relaxation data of pressure-densified PMMA and PS has shown that these glasses are less stable than nondensified ones because, with increasing formation pressure, their hysteresis peak temperature increased and the peak height decreased. To account for these results, Weitz and Wunderlich assumed a freezing of high-energy conformations, mainly connected with higher enthalpy, and a freezing of holes, connected with lower enthalpy and lower volume, which would then result in memory-effect-like relaxations to more stable and denser states. Similarly, a reduction in density fluctuation in pressure-densified PS glasses[33] has led to the conlusion that, in these glasses, unfavorable chain conformations are trapped in local energy minima that can then promote segmental motion leading to volume expansion even far below T_g. In a more recent paper, Song and Roe[44] have demonstrated, in a detailed small and intermediate angle X-ray scattering study of PS, that pressure-densified glasses exhibit greatly reduced local ordering compared with physically aged glasses, despite their much higher densities. They have therefore suggested that the mechanical relaxation times of glasses are determined not only by the free volume content but also by the state of local packing of segments.

Conclusions

We have summarized different pressure−volume−temperature (PVT) formation paths that can be used

to obtain densified polymer glasses and concluded that pressure densification in the equilibrium melt is the preferred formation path. Our modified sample cell can be used together with a commercial *PVT* apparatus to make isotropic pressure-densified samples of polymer glasses. Silicone oil was used as a pressure-transmitting fluid and could be removed almost completely from the sample surface using *n*-hexane or diethyl ether as revealed by electron spectroscopy for chemical analysis (ESCA). We have thus made a number of pressure-densified atactic poly(methyl methacrylate) (*a*-PMMA) glasses with formation pressures in the equilibrium melt in the range of 0−200 MPa or 1.1823−1.1963 g/cm^3 for further analysis with positron annihilation lifetime spectroscopy (PALS). Cross-polarized light microscopy confirmed that the glasses were isotropic.

We have measured the *PVT* properties of the glasses and the melt using thermodynamically and chemically identical specimens and have discussed all results in terms of the Simha−Somcynsky equation-of-state (EOS) theory and the Tait EOS. The *PVT* data are shown to be self-consistent as well as in very good agreement with literature data. Moreover, our *PVT* data and the EOS analysis extend the range of densification pressure up to 200 MPa compared with previously investigated pressure-densified glasses. We thus find that, at RT and atmospheric pressure, (a) the macroscopic volume decreases by up to 1.2%, (b) the free-volume fraction h from the Simha−Somcynsky theory decreases by up to 19.2%, and (c) the freezing fraction of pressure-densified glasses is invariant up to a formation pressure of 200 MPa. The corresponding microscopic volume changes from PALS were an 8.4% decrease in orthopositronium (o-Ps) lifetime τ_3 and a 16.1% decrease of the free-volume hole size $V(\tau_3)$. We therefore conclude that small macroscopic volume changes yield large microscopic volume changes in pressure-densified *a*-PMMA glasses. Moreover, we conclude that h correlates best with $V(\tau_3)$ and tentatively suggest that this correlation indicates that the radius of the free-volume cavities $R(\tau_3)$ at zero h is close to the Bohr diameter of the o-Ps species. From the o-Ps intensity I_3 of the glasses, we conclude that I_3 is independent of formation pressure.

Acknowledgment. We are grateful to Mattias Olsson for the second set of PALS data, Ann Wendel for ESCA measurements, Anders Mårtensson for optical micrographs and the technical drawing, and Henrik Ramebäck for preparation of the PALS source. This work was supported by the Swedish Research Council for Engineering Sciences (TFR).

References and Notes

(1) O'Reilly, J. M. In *Modern Aspects of the Vitreous State*; Mackenzie, J. D., Ed.; Butterworth: London, 1964; Vol. 3, pp 59−89.
(2) Zoller, P. In *Polymer Handbook*, 3rd ed.; Brandrup, J., Immergut, E. H., Eds.; Wiley: New York, 1989; Vol. VI, pp 475−483.
(3) Zoller, P.; Walsh, D. J. *Standard Pressure−Volume−Temperature Data for Polymers*, 1st ed.; Technomic Publishing Co. Inc.: Lancaster, 1995; pp 1−17.
(4) Schmidt, M.; Maurer, F. H. J. *J. Polym. Sci., Part B: Polym. Phys.* **1998**, *36*, 1061−1080.
(5) Struik, L. C. E. *Physical Aging in Amorphous Polymers and Other Materials*; Elsevier: Amsterdam, 1978; pp 31−32, 176.
(6) Vernel, J.; Rychwalski, R. W.; Pelísek, V.; Sáha, P.; Schmidt, M.; Maurer, F. H. J. *Thermochim. Acta* **1999**, *342*, 115−137.
(7) Kovacs, A. J. *J. Polym. Sci.* **1958**, *30*, 131−147.
(8) Greiner, R.; Schwarzl, F. R. *Rheol. Acta* **1984**, *23*, 378−395.
(9) Goldstein, M. *J. Phys. Chem.* **1973**, *77*, 667−673.
(10) Yourtee, J. B.; Cooper, S. L. *J. Appl. Polym. Sci.* **1974**, *18*, 897−912.
(11) McKinney, J. E.; Goldstein, M. *J. Res. Nat. Bur. Stand., Part A: Phys. Chem.* **1974**, *78A*, 331−353.
(12) Tammann, G.; Jenckel, E. *Z. Anorg. Allg. Chem.* **1929**, *184*, 416−420.
(13) Shishkin, N. I.; Kovalichev, O. F. *Sov. Phys. (Solid State)* **1960**, *2*, 329−331.
(14) Shishkin, N. I. *Sov. Phys. (Solid State)* **1960**, *2*, 322−328.
(15) O'Reilly, J. *J. Polym. Sci.* **1962**, *57*, 429−444.
(16) Breuer, H.; Rehage, G. *Kolloid Z. Z. Polym.* **1967**, *216−217*, 159−179.
(17) Rehage, G.; Breuer, H. *J. Polym. Sci., Part C* **1967**, *16*, 2299−2312.
(18) Kimmel, R. M.; Uhlmann, D. R. *J. Appl. Phys.* **1970**, *41*, 2917−2927.
(19) Ichihara, S.; Komatsu, A.; Tsujita, Y.; Nose, T.; Hata, T. *Polym. J.* **1971**, *2*, 530−534.
(20) Quach, A.; Simha, R. *J. Appl. Phys.* **1971**, *42*, 4592−4606.
(21) Kimmel, R. M.; Uhlmann, D. R. *J. Appl. Phys.* **1971**, *42*, 1892.
(22) Quach, A.; Simha, R. *J. Phys. Chem.* **1972**, *76*, 416−421.
(23) Dale, W. C.; Rogers, C. E. *J. Appl. Polym. Sci.* **1972**, *16*, 21−36.
(24) Weitz, A.; Wunderlich, B. *J. Polym. Sci., Part B: Polym. Phys.* **1974**, *12*, 2473−2491.
(25) Bree, H. W.; Heijboer, J.; Struik, L. C. E.; Tak, A. G. M. *J. Polym. Sci., Part B: Polym. Phys.* **1974**, *12*, 1857−1864.
(26) Olabisi, O.; Simha, R. *Macromolecules* **1975**, *8*, 206−210.
(27) Price, C. *Polymer* **1975**, *16*, 585−589.
(28) Wetton, R. E.; Moneypenny, H. G. *Br. Polym. J.* **1975**, *7*, 51−68.
(29) Oels, H.-J.; Rehage, G. *Macromolecules* **1977**, *10*, 1036−1043.
(30) Brown, I. G.; Wetton, R. E.; Richardson, M. J.; Savill, N. G. *Polymer* **1978**, *19*, 659−663.
(31) Lee, H.; Jamieson, A. M.; Simha, R. *Colloid Polym. Sci.* **1980**, *258*, 545−555.
(32) Naoki, M.; Mori, H.; Owada, A. *Macromolecules* **1981**, *14*, 1567−1575.
(33) Curro, J. J.; Roe, R. J. *J. Polym. Sci., Polym. Phys. Ed.* **1983**, *21*, 1785−1796.
(34) Robertson, R. E.; Simha, R.; Curro, J. G. *Macromolecules* **1985**, *18*, 2239−2246.
(35) Gee, G. *Polymer* **1966**, *7*, 177−191.
(36) Kimmel, R. M.; Uhlmann, D. R. *J. Appl. Phys.* **1971**, *42*, 4917−4925.
(37) Nose, T. *Polym. J.* **1971**, *2*, 445−456.
(38) Olabisi, O.; Simha, R. *Macromolecules* **1975**, *8*, 211−218.
(39) Papazoglou, E.; Simha, R. *Macromolecules* **1988**, *21*, 1670−1677.
(40) Destruel, P.; Ai, B.; Hoang The, G. *J. Polym. Sci., Part B: Polym. Phys.* **1983**, *21*, 851−858.
(41) Destruel, P.; Ai, B.; Hoang The, G. *J. Appl. Phys.* **1984**, *55*, 2726−2732.
(42) Schmidt, M.; Brodin, A.; Jacobsson, P.; Maurer, F. H. J. *J. Chem. Phys.* **2000**, *112*, 1020−1028.
(43) Simha, R.; Jain, S. C.; Jamieson, A. M. *Macromolecules* **1982**, *15*, 1517−1521.
(44) Song, H. H.; Roe, R. J. *Macromolecules* **1987**, *20*, 2723−2732.
(45) Coakley, R. W.; Hunt, J. L.; Stevens, J. R. *J. Appl. Phys.* **1983**, *54*, 5603−5607.
(46) McKinney, J. E.; Simha, R. *Macromolecules* **1974**, *7*, 894−901.
(47) McKinney, J. E.; Simha, R. *Macromolecules* **1976**, *9*, 430−441.
(48) Gee, G. *Contemp. Phys.* **1970**, *11*, 313−334.
(49) Ferry, J. D. *Viscoelastic Properties of Polymers*, 3rd ed.; John Wiley & Sons: New York, 1980; pp 291−298.
(50) Tsirule, K. I.; Tyunina, E. L. In *High-Pressure Chemistry and Physics of Polymers*; Kovarskii, A. L., Ed.; CRC Press: London, 1994; pp 1−22.
(51) Tsirule, K. I.; Tyunina, E. L. In *High-Pressure Chemistry and Physics of Polymers*; Kovarskii, A. L., Ed.; CRC Press: London, 1994; pp 59−115.
(52) McKinney, J. E.; Simha, R. *J. Res. Nat. Bur. Stand., Part A: Phys. Chem.* **1977**, *81A*, 283−297.
(53) Struik, L. C. E. *Internal Stresses, Dimensional Instabilities and Molecular Orientations in Plastics*; John Wiley & Sons: New York, 1990; pp 17−19.
(54) Vleeshouwers, S.; Nies, E. *Thermochim. Acta* **1994**, *238*, 371−395.
(55) Kobayashi, Y. *Ber. Bunsen-Ges. Phys. Chem.* **1992**, *97*, 1869−1872.

(56) Wilson, R. K.; Johnson, P. O.; Stump, R. *Phys. Rev.* **1963**, *129*, 2091−2095.
(57) Wang, Y. Y.; Nakanishi, H.; Jean, Y. C.; Sandreczki, T. C. *J. Polym. Sci., Part B: Polym. Phys.* **1990**, *28*, 1431−1441.
(58) Hugenschmidt, C.; Maier, K. *Mater. Sci. Forum* **1997**, *255−257*, 467−471.
(59) Kobayashi, Y.; Haraya, K.; Hattori, S.; Sasuga, T. *Polymer* **1994**, *35*, 925−928.
(60) Hong, X.; Jean, Y. C.; Yang, H.; Jordan, S. S.; Koros, W. J. *Macromolecules* **1996**, *29*, 7859−7864.
(61) Ito, Y. *Polym. Mater. Sci. Eng.* **1997**, *76*, 425−427.
(62) Simha, R.; Somcynsky, T. *Macromolecules* **1969**, *2*, 342−350.
(63) Nanda, V. S.; Simha, R. *J. Chem. Phys.* **1964**, *21*, 1884−1885.
(64) Somcynsky, T.; Simha, R. *J. Appl. Phys.* **1971**, *42*, 4545−4548.
(65) Yi, Y. X.; Zoller, P. *J. Polym. Sci., Part B: Polym. Phys.* **1993**, *31*, 779−788.
(66) Simha, R. *Macromolecules* **1977**, *10*, 1025−1030.
(67) Simha, R.; Wilson, P. S. *Macromolecules* **1973**, *6*, 908−914.
(68) Ache, H. J. In *Positron and Positronium Chemistry*; Schrader, D. M., Yean, Y. C., Eds.; Elsevier: Amsterdam, 1988; Vol. 57, pp 318−352.
(69) Wang, S. J.; Jean, Y. C. In *Positron and Positronium Chemistry*; Schrader, D. M., Yean, Y. C., Eds.; Elsevier: Amsterdam, 1988; Vol. 57, pp 255−281.
(70) Welander, M.; Maurer, F. H. J. *Mater. Sci. Forum* **1992**, *105−110*, 1811−1814.
(71) Kluin, J. E.; Moaddel, H.; Ruan, M. Y.; Yu, Z.; Jamieson, A. M.; Simha, R.; McGervey, J. D. *Adv. Chem. Ser.* **1993**, *236*, 535−555.
(72) Jean, Y. C. *Mater. Sci. Forum* **1995**, *175−178*, 59−70.
(73) Hill, A. J. In *High-Temperature Properties and Applications of Polymeric Materials*; Tant, M. R., Connell, J. W., McManus, L. N., Eds.; American Chemical Society: Washington, DC, 1995; pp 63−80.
(74) Wang, C. L.; Hirade, T.; Maurer, F. H. J.; Eldrup, M.; Pedersen, N. J. *J. Chem. Phys.* **1998**, *108*, 1−8.
(75) Dammert, R. M.; Maunu, S. L.; Maurer, F. H. J.; Neelov, I. M.; Niemelä, S.; Sundholm, F.; Wästlund, C. *Macromolecules* **1999**, *32*, 1930−1938.
(76) Schrader, D. M.; Jean, Y. C. In *Positron and Positronium Chemistry*; Schrader, D. M., Jean, Y. C., Eds.; Elsevier: Amsterdam, 1988; Vol. 57, pp 1−26.
(77) Mogensen, O. E. *Positron Annihilation in Chemistry*; Goldanskii, V. I., Schäfer, F. P., Toennies, J. P., Eds.; Springer-Verlag: Berlin, 1995; Vol. 58, pp 1−9.
(78) Brandt, W.; Berko, S.; Walker, W. W. *Phys. Rev.* **1960**, *120*, 1289−1295.
(79) Tao, S. J. *J. Chem. Phys.* **1972**, *56*, 5499−5510.
(80) Eldrup, M.; Lightbody, D.; Sherwood, J. N. *Chem. Phys.* **1981**, *63*, 51−58.
(81) Nakanishi, H.; Jean, Y. C. In *Positron and Positronium Chemistry*; Schrader, D. M., Yean, Y. C., Eds.; Elsevier: Amsterdam, 1988; Vol. 57, pp 159−192.
(82) Gregory, R. B. *J. Appl. Phys.* **1991**, *70*, 4665−4670.
(83) Jean, Y. C.; Deng, Q. *J. Polym. Sci., Part B: Polym. Phys.* **1992**, *30*, 1359−1364.
(84) Okamoto, K.; Tanaka, K.; Katsube, M.; Kita, H.; Ito, Y. *Bull. Chem. Soc. Jpn.* **1993**, *66*, 61−68.
(85) Yu, Z.; McGervey, J. D.; Jamieson, A. M.; Simha, R. *Macromolecules* **1995**, *28*, 6268−6272.
(86) Jean, Y. C. *Macromolecules* **1996**, *29*, 5756−5757.
(87) Baugher, A. H.; Kossler, W. J.; Petzinger, K. G. *Macromolecules* **1996**, *29*, 7280−7283.
(88) Wang, C. L.; Maurer, F. H. J. *Macromolecules* **1996**, *29*, 8249−8253.
(89) Wästlund, C.; Maurer, F. H. J. *Nucl. Instrum. Methods Phys. Res. B* **1996**, *117*, 467−473.
(90) Dlubek, G.; Eichler, S. *Phys. Status Solidi A* **1998**, *168*, 333−350.
(91) Shukla, A.; Peter, M.; Hoffmann, L. *Nucl. Instrum. Methods Phys. Res. A* **1993**, *335*, 310−317.
(92) Shukla, A.; Hoffmann, L.; Manuel, A. A.; Peter, M. *Mater. Sci. Forum* **1997**, *255−257*, 233−237.
(93) Kobayashi, Y.; Zheng, W.; Meyer, E. F.; McGervey, J. D.; Jamieson, A. M.; Simha, R. *Macromolecules* **1989**, *22*, 2302−2306.
(94) Wästlund, C.; Maurer, F. H. J. *Polymer* **1998**, *39*, 2897−2902.
(95) Suzuki, T.; Miura, T.; Oki, Y.; Numajiri, M.; Kondo, K.; Ito, Y. *Radiat. Phys. Chem.* **1995**, *45*, 657−663.
(96) Peng, Z. L.; Olson, B. G.; McGervey, J. D.; Jamieson, A. M. *Polymer* **1999**, *40*, 3033−3040.
(97) Hirade, T.; Maurer, F. H. J.; Eldrup, M. *Radiat. Phys. Chem.*, in press.
(98) Ito, Y. In *Positron and Positronium Chemistry*; Schrader, D. M., Yean, Y. C., Eds.; Elsevier: Amsterdam, 1988; Vol. 57, pp 120−158.
(99) Kobayashi, Y.; Wang, C. L.; Hirata, K.; Zheng, W.; Zhang, C. *Phys. Rev. B: Condens. Matter Mater. Phys.* **1998**, *58*, 5384−5389.
(100) Schrader, D. M. In *Positron and Positronium Chemistry*; Schrader, D. M., Jean, Y. C., Eds.; Elsevier: Amsterdam, 1988; Vol. 57, pp 27−90.
(101) Schmidt, M.; Maurer, F. H. J. *Polymer*, in press.
(102) Zoller, P.; Bolli, P.; Pahud, V.; Ackermann, H. *Rev. Sci. Instrum.* **1976**, *47*, 948−952.
(103) Lei, M.; Reid, C. G.; Zoller, P. *Polymer* **1988**, *29*, 1784−1788.
(104) Gnomix *PVT Manual*, Version 6.0; Gnomix Inc.: Boulder, CO, 1991−1993.
(105) Fuchs, O. In *Polymer Handbook*, 3rd ed.; Brandrup, J., Immergut, E. H., Eds.; John Wiley & Sons: New York, 1989; Vol. VII, pp 379−407.
(106) PATFIT-1988 *Computer Program*: Risø National Laboratory, Denmark.
(107) Kressler, J.; Higashida, N.; Shimomai, K.; Inoue, T.; Ougizawa, T. *Macromolecules* **1994**, *27*, 2448−2453.
(108) Rodgers, P. A. *J. Appl. Polym. Sci.* **1993**, *48*, 1061−1080.
(109) Simha, R.; Wilson, P. S.; Olabisi, O. *Kolloid Z. Z. Polym.* **1973**, *251*, 402−408.
(110) Hellwege, K.-H.; Knappe, W.; Lehmann, P. *Kolloid Z. Z. Polym.* **1962**, *183*, 110−120.
(111) Haldon, R.; Simha, R. *J. Appl. Phys.* **1968**, *39*, 1890−1899.
(112) Rogers, S. S.; Mandelkern, L. *J. Phys. Chem.* **1957**, *61*, 985−990.
(113) Simha, R.; Boyer, R. F. *J. Chem. Phys.* **1962**, *37*, 1003−1007.
(114) Bauwens, J.-C. *Polymer* **1980**, *21*, 699−705.
(115) Wästlund, C.; Eldrup, M.; Maurer, F. H. J. *Nucl. Instrum. Methods Phys. Res. B* **1998**, *143*, 575−583.
(116) Hasan, O. A.; Boyce, M. C.; Li, X. S.; Berko, S. *J. Polym. Sci., Part B: Polym. Phys.* **1993**, *31*, 185−197.
(117) Ruan, M. Y.; Moaddel, H.; Jamieson, A. M.; Simha, R.; McGervey, J. D. *Macromolecules* **1992**, *25*, 2407−2411.
(118) Robertson, C. G.; Wilkes, G. L. *Polymer* **1998**, *39*, 2129−2133.

MA991722H